Journal Pre-proofs

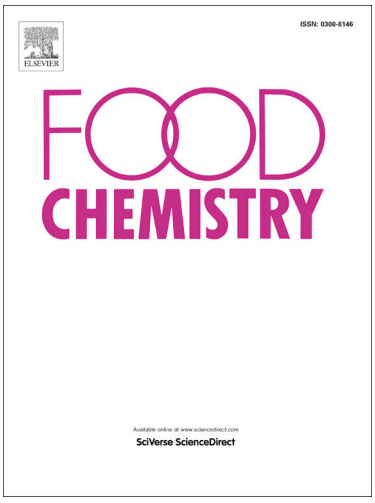

Characterization of Chemical Composition and Prebiotic Effect of a Dietary Medicinal Plant *Penthorum Chinense* Pursh

Jianhua Yin, Wei Ren, Bin Wei, Huimin Huang, Mingxing Li, Xiaoxiao Wu, Anqi Wang, Zhangang Xiao, Jing Shen, Yueshui Zhao, Fukuan Du, Huijiao Ji, Parham Jabbarzadeh Kaboli, Yongshun Ma, Zhuo Zhang, Chi Hin Cho, Shengpeng Wang, Xu Wu, Yitao Wang

PII: S0308-8146(20)30430-1
DOI: https://doi.org/10.1016/j.foodchem.2020.126568
Reference: FOCH 126568

To appear in: *Food Chemistry*

Received Date: 10 January 2020
Revised Date: 4 March 2020
Accepted Date: 4 March 2020

Please cite this article as: Yin, J., Ren, W., Wei, B., Huang, H., Li, M., Wu, X., Wang, A., Xiao, Z., Shen, J., Zhao, Y., Du, F., Ji, H., Jabbarzadeh Kaboli, P., Ma, Y., Zhang, Z., Hin Cho, C., Wang, S., Wu, X., Wang, Y., Characterization of Chemical Composition and Prebiotic Effect of a Dietary Medicinal Plant *Penthorum Chinense* Pursh, *Food Chemistry* (2020), doi: https://doi.org/10.1016/j.foodchem.2020.126568

Characterization of Chemical Composition and Prebiotic Effect of a Dietary Medicinal Plant *Penthorum Chinense* Pursh

Jianhua Yin[a,b,1], Wei Ren[c,1], Bin Wei[d,1], Huimin Huang[a,b], Mingxing Li[a,b], Xiaoxiao Wu[a,b], Anqi Wang[e], Zhangang Xiao[a,b], Jing Shen [a,b], Yueshui Zhao[a,b], Fukuan Du[a,b], Huijiao Ji[a,b], Parham Jabbarzadeh Kaboli[a,b], Yongshun Ma[a,b], Zhuo Zhang[a,b], Chi Hin Cho[a,b], Shengpeng Wang[f,*], Xu Wu[a,b,*] Yitao Wang[f]

[a] *Laboratory of Molecular Pharmacology, Department of Pharmacology, School of Pharmacy, Southwest Medical University, Luzhou, Sichuan, China*

[b] *South Sichuan Institute of Translational Medicine, Luzhou, Sichuan, China*

[c] *Drug Research Center of Integrated Traditional Chinese and Western Medicine, Affiliated Traditional Chinese Medicine Hospital, Southwest Medical University, Luzhou, Sichuan, China*

[d] *College of Pharmaceutical Science & Collaborative Innovation Center of Yangtze River Delta Region Green Pharmaceuticals, Zhejiang University of Technology, Hangzhou, China*

[e] *PU-UM Innovative Institute of Chinese Medical Sciences, Guangdong-Macau Traditional Chinese Medicine Technology Industrial Park Development Co., Ltd, Hengqin New Area, Zhuhai, Guangdong, China*

[f] *State Key Laboratory of Quality Research in Chinese Medicine, Institute of Chinese Medical Sciences, University of Macau, Macao, China*

[1] *These authors contributed equally to this work.*

*Corresponding authors.

Xu Wu, Laboratory of Molecular Pharmacology, Department of Pharmacology, School of Pharmacy, Southwest Medical University, Luzhou 646000, Sichuan, China. Tel: +86-13882770623. E-mail: wuxulz@126.com.

Shengpeng Wang, State Key Laboratory of Quality Research in Chinese Medicine, Institute of Chinese Medical Sciences, University of Macau, Macao, China. Tel: +86-15344896403, E-mail: swang@um.edu.mo.

Abstract

Penthorum chinense Pursh is a dietary medicinal plant widely distributed in Asia-Pacific countries. The present study aimed to profile the chemical constituents of *P. chinense* and investigate its prebiotic role in modulating gut microbiota. Fifty

polyphenolic compounds were rapidly identified using UPLC-HR-MS. Total flavonoid and phenolic contents of *P. chinense* were 46.6% and 61.3% (*w/w*), respectively. Thirteen individual polyphenols were quantified, which accounted for 33.1% (*w/w*). *P. chinense* induced structural arrangement of microbial community in mice, showing increased microbiota diversity, elevated *Bacteroidetes*/*Firmicutes* ratio and enriched gut health-promoting bacteria. After a one-week drug-free wash, most of these changes were recovered, but the abundance of some beneficial bacteria was further increased. The altered composition of gut microbiota enriched several metabolic pathways. Moreover, *P. chinense* increased antioxidant capacity *in vivo*. The results suggest that polyphenol-enriched *P. chinense* modulates gut microbiota and enhances antioxidant capacity in mice toward a beneficial environment for host health.

Keywords: *Penthorum chinense*; mass spectrometry; polyphenol; gut microbiota; prebiotics; antioxidant

Chemicals: Quercetin (PubChem CID: 5280343), Quercetin-3-*O*-Glucoside (PubChem CID: 5280804), Quercetin-3-*O*-Arabinfuranoside (PubChem CID: 5481224), Quercetin-3-*O*-Rhamnoside (PubChem CID: 5280459), Kaempferol (PubChem CID: 5280863), Kaempferol-3-*O*-Rutinoside (PubChem CID: 5318767), Pinocembrin (PubChem CID: 68071), Thonningianin A (PubChem CID: 10328286), Gallic Acid (PubChem CID: 370), Brevifolin Carboxylic Acid (PubChem CID: 9838995).

Abbreviations： ALD, alcoholic liver disease; CAT, catalase; ESI, electrospray

ionization; GSH, glutathione; GSH-Px, glutathione peroxidase; KEGG, Kyoto Encyclopedia of Genes and Genomes; LDA, linear discriminant analysis; LEfSe, linear discriminant analysis effect size; NALD, non-alcoholic liver disease; NASH, non-alcoholic steatohepatitis; OUT, operational taxonomic unit; PCoA, principal co-ordinates analysis; PLS-DA, partial least squares discriminant analysis; SCFA, short-chain fatty acid; SOD, superoxide dismutase; T-AOC, total antioxidant capacity; UPLC-HR-MS, ultra high-performance liquid chromatography coupled with high resolution mass spectrometry.

1. Introduction

A diverse and complex microbial community residing in intestinal tract, a hidden metabolic organ, plays an important role in human health (Guinane & Cotter, 2013). Dysbiosis of gut microbiota has been associated with pathogenesis of many metabolic diseases including inflammatory bowel disease, chronic liver disease, obesity as well as diabetes (Carding, Verbeke, Vipond, Corfe, & Owen, 2015). It is widely acknowledged that diet significantly impacts host health and disease status in both direct and indirect ways. Dietary modulation of gut microbiota is increasingly believed as a promising approach for treatment of gut microbiota-associated diseases. Notably, polyphenol-enriched herbal products (*e.g.*, grape seed extract, red wine, and green tea) have long been reported to have a protective effect against metabolic syndromes (Bose, Lambert, Ju, Reuhl, Shapses, & Yang, 2008). Polyphenols are usually of very low bioavailability, however, many recent studies have suggested that polyphenols (*e.g.*,

silymarins, ellagitannins, resveratrol, and curcumin) modulated gut microbiota resulting in a beneficial environment to produce anti-inflammatory metabolites and promote host health (Selma, Espin, & Tomasbarberan, 2009). The prebiotic potential of polyphenols or polyphenol-enriched extracts is attracting increasing research attentions.

Penthorum chinense Pursh (*P. chinense*) is a medicinal plant of *Penthoraceae* family which is widely used in China for prevention and treatment of liver diseases such as alcoholic and non-alcoholic fatty liver and hepatitis (Wang et al., 2020). It is as well often applied in functional drink or as a vegetable by the locals. It has been prepared into standard extract in China and is available in market under the trademark of "Gansu" for treating chronic liver disease. Over 80 compounds including flavonoids, phenylpropanoids, organic acids and phenols (all belonging to polyphenols) have been identified from *P. chinense* (Wang et al., 2020). Pharmacological and biomedical experiments demonstrate that *P. chinense* has a protective role in animal models of alcoholic and nonalcoholic liver disease, liver fibrosis and chemical-induced liver injury potentially through exerting effects of antioxidation, anti-inflammation, as well as inhibition of stellate cell activation (Wang et al., 2020). Although *P. chinense* is a promising liver-protecting candidate for further research and development, however, both the chemical compositions and action mechanisms remain unclear in most parts. Therefore, the present study aims to rapid profile chemical constituents of *P. chinense* based on ultra high-performance liquid chromatography coupled with high resolution

mass spectrometry (UPLC-HR-MS) and to investigate whether and how *P. chinense* as a dietary product impacts gut microbiota in mice. The results will provide evidences on active principals and potential action mechanisms of *P. chinense*.

2. Materials and methods

2.1. Materials and Reagents

Acetonitrile, methanol and formic acid (HPLC grade) were obtained from Merck. Distilled water was prepared from Milli-Q system (Millipore, USA). Reference standards of quercetin, quercetin-3-*O*-glucoside, quercetin-3-*O*-arabinfuranoside, quercetin-3-*O*-rhamnoside, kaempferol, kaempferol-3-*O*-rutinoside, pinocembrin, thonningianin A, pinocembrin-7-*O*-[3"-*O*-galloyl-4",6"-hexahydroxydiphenoyl]-glucoside, catechin, epicatechin, rutin, luteolin, apigenin, gallic acid, bergenin, brevifolin carbocylic acid, and ethyl gallate (purity > 98%) were purchased from Chengdu Must Bio-Technology Co., Ltd.

The whole grass of *P. chinense* was obtained from Neautus Traditional Chinese Medicine Co., Ltd (Sichuan, China), and identified by Prof. Jin Pei, Chengdu University of Traditional Chinese Medicine. A voucher specimen was deposited at the herbarium of Institute of Chinese Medical Sciences, University of Macau. The preparation procedure is described previously (Wang, Wang, Jiang, Chen, Wang, & Lin, 2016), which was consistent with its standard extraction procedure documented in Standards of Ministry of Health for Chinese Medicinal Preparations. In brief, the dried whole grass of *P. chinense* was ground into powder and extracted with boiling water

for three times (2 h for each time). After the concentration of the resulting decoction to a small volume, ethanol was added until 60% to precipitate the high-molecule proteins and polysaccharides for three times. Then the supernatant was collected and lyophilized to yield the dried *P. chinense* extract.

2.2. UPLC-HR-MS for chemical characterization

The ultimate 3000 hyperbaric LC system coupled with high resolution Orbitrap Fusion Lumos Tribrid™ via an electrospray ionization (ESI) interface from Thermo Fisher Scientific (Bremen, Germany) was used for a comprehensive analysis of the constituents in *P. chinense* extract. The chromatography system was equipped with an auto-sampler, a diode-array detector, a column compartment, and two pumps. The chromatographic conditions were optimized and a BEH C18 column (1.7 μm, 2.1 mm ID × 100 mm, Waters) maintained at 35 °C was finally chosen for separation of *P. chinense* extract. The mobile phase was composed of water (0.1% formic acid, A) mixed in gradient mode with acetonitrile (0.1% formic acid, B), at a flow rate of 200 μL/min. The elution gradient was optimized as follows: 0-3 min, 3% B; 3-6 min, 3% to 25% B; 6-28 min, 25% to 42% B; 28-30 min, 42% to 100% B; 30-32 min, 100% B. The injection volume was 3.0 μL and the sampler was set at 4 °C.

For identification of the components in *P. chinense* extract, positive full scan modes within the range of *m/z* (mass/charge ratio) 150-1500 at a resolution of 120,000 were used for acquisition of accurate molecular ion. The other parameters were set as follows: spray voltage, +3.0 kV; sheath gas flow rate, 35 arb; aux gas flow rate, 10 arb; sweep

gas, 2 arb; capillary temperature, 320 °C; vaporizer temperature, 250 °C; RF lens, 50%. The fragment ions in MS/MS data obtained by higher energy collision dissociation (HCD) at proper collision energy were further utilized for confirmation of the structures of the components. In addition, standards were also used for assistance of identification of the components. Xcalibur 3.0 software (Thermo Fisher) was used for UPLC-HR-MS control and data handling.

2.3. Determination of total flavonoid and phenolic contents

Total flavonoid and phenolic contents were performed using $NaNO_2$/ $AlCl_3$/ NaOH and Folin-Ciocalteu method, respectively, both according to the protocols reported by (Orsavová, Hlaváčová, Mlček, Snopek, & Mišurcová, 2019) using the respective standard of rutin and gallic acid. Cytation 3 Multi-Mode Reader (BioTek) was used for the detection. Results were expressed as grams of rutin equivalent (RE)/g of extract (g RE/g) and as grams of gallic acid equivalent (GAE)/g of extract (g GAE/g), respectively.

2.4. UPLC-QqQ-MS for quantitative analysis

2.4.1. LC-MS/MS condition

A Shimadzu Nexera UPLC tandem LCMS-8045 triple quadrupole (QqQ) mass spectrometry was used. Chromatographic separation was achieved on a Shim-pack XR-ODSII C18 column (2.0×100 mm, 2.2 μm) coupled with a Shim-pack GIST-HP(G) C18 Guard column (1.5×10 mm, 2 μm). The mobile phase system included water (0.1% formic acid, A) and acetonitrile (0.1% formic acid, B). The eluting gradient was as

follows: 0-0.5 min, 0% B，0.5-1.20 min 0-5% B, 1.20-6.00 min 5-50% B, 6.00-11.00 min 50-100% B, 11.00-12.00 min 100% B, 12.01 min 100-0% B, 12.01-14.00 min 0% B. The flow rate was set at 200 μL/min. The injection volume and column temperature were 10 μL and 35 ℃, respectively.

The quantitation was optimized and performed in multiple reaction monitoring (MRM) mode. The mass spectrometer was operated at the following condition: Spary (N_2), 4 L/min; Heat Gas Flow, 11 L/min; Dry Gas, 11 L/min; Interface Temp, 340 ℃; DL, 300 ℃; Heat Block Temp, 350 ℃; Interface Voltage, 4 kV. The MRM parameters (Ion pair, retention time, Q1 Pre, Collision Energy, and Q3 Pre) for each analyte are displayed in supplementary Table 1.

2.4.2. Sample preparation

P. chinense extract (10 mg) was accurately weighed and dissolved in 50% methanol with sonication for 2 min. The solution was further filtrated through 0.22 μm membrane for LC-MS/MS analysis.

2.4.3. Method validation

The quantitative method was validated with linearity, limit of detection (LOD), limit of quantification (LOQ), precision, accuracy, and recovery. The linearity of each analyte was established by plotting peak area of analyte against serial designated concentrations. The LOD and LOQ were determined at concentrations with the signal-to-noise (S/N) ratio of 3 and 10. The precision and accuracy of the methods were determined by

repeated analysis of a standard solution within 24 h. The precision was evaluated by the RSD value with replicate assays (n = 6), and the accuracy (n = 6) was evaluated based on the error of the assayed standard solution relative to the nominal concentrations. The stability of standard solution of analytes was determined by a repeated analysis at 0, 2, 4, 8, 12, and 24 h. To evaluate recovery, known amounts of each analyte were spiked into *P. chinense* extract, which was further extracted as described in sample preparation part for LC-MS/MS analysis. The results of method validation are displayed in supplementary Table 2 and supplementary Table 3, which suggested the suitability and robustness of the developed method for the quantification process.

2.5. Microbial diversity analysis

2.5.1. Sample collection

The care of animals and all experimental procedures were approved by the Committee on Use and Care of Animals of Southwest Medical University. SPF Male C57BL/6J mice (18-20 g) supplied by the Hua-Fu-Kang Biotechnologies (Beijing, China) were maintained under controlled conditions of temperature (22-24 ^{o}C), humidity (55-60 %), and a light/dark cycle of 12/12 h.

Before the start of experiment, all mice were allowed *ad libitum* access to food sterilized by ^{60}Co irradiation from Dashuo Biotechnologies (Chengdu, China) and autoclaved water for accommodation in the first 2 weeks. Food was given at 17:00-18:00 p.m. of each day to avoid disturbance of the circadian clock. Mice (n = 10) were administered

with *P. chinense* extract at a dosage of 0.4 g (equivalent to 4 g crude herb)/kg via *p.o.* for 5 consecutive days (day 1-5) at 9:00-10:00 a.m. of each day. Fresh fecal specimens of all mice were collected at day 0, 6 and 13, respectively. Fecal specimens were collected at 15:00-17:00 p.m. to minimize possible circadian effects. Samples were placed into empty sterilized microtubes on ice and stored at -80 °C within 1 h after collection.

2.5.2. DNA extraction and PCR amplification

Microbial DNA was extracted from mice fecal samples using the E.Z.N.A.® soil DNA Kit (Omega Bio-tek, Norcross, GA, U.S.) according to manufacturer's protocols. The final DNA concentration and purification were determined by NanoDrop 2000 UV-vis spectrophotometer (Thermo Scientific, Wilmington, USA), and DNA quality was checked by 1% agarose gel electrophoresis. The V3-V4 hypervariable regions of the bacteria 16S rRNA gene were amplified with primers 338F (5'-ACTCCTACGGGAGGCAGCAG-3') and 806R (5'-GGACTACHVGGGTWTCTAAT-3') by thermocycler PCR system (GeneAmp 9700, ABI, USA). PCR reactions were performed in triplicate 20 μL mixture containing 4 μL of 5 × FastPfu Buffer, 2 μL of 2.5 mM dNTPs, 0.8 μL of each primer (5 μM), 0.4 μL of FastPfu Polymerase and 10 ng of template DNA. The resulted PCR products were extracted from a 2% agarose gel and further purified using the AxyPrep DNA Gel Extraction Kit (Axygen Biosciences, Union City, CA, USA) and quantified using QuantiFluor™-ST (Promega, USA) according to the manufacturer's protocol.

2.5.3. Illumina MiSeq sequencing

Purified amplicons were pooled in equimolar and paired-end sequenced (2 × 300) on an Illumina MiSeq platform (Illumina, San Diego, USA) according to the standard protocols by Majorbio Bio-Pharm Technology Co. Ltd. (Shanghai, China).

2.5.4. Processing of sequencing data

Analysis of the gut microbial community was carried out using the free online platform of Majorbio Cloud Platform (www.majorbio.com). Raw fastq files were demultiplexed, quality-filtered by Trimmomatic and merged by FLASH with the following criteria: (i) The reads were truncated at any site receiving an average quality score < 20 over a 50 bp sliding window. (ii) Primers were exactly matched allowing 2 nucleotide mismatching, and reads containing ambiguous bases were removed. (iii) Sequences whose overlap longer than 10 bp were merged according to their overlap sequence.

Operational taxonomic units (OTUs) were clustered with 97% similarity cut off using UPARSE (version 7.1, http://drive5.com/uparse/) and chimeric sequences were identified and removed using UCHIME. The taxonomy of each 16S rRNA gene sequence was analyzed by RDP Classifier algorithm (http://rdp.cme.msu.edu/) against the Silva (SSU123) 16S rRNA database using confidence threshold of 70%.

Rarefaction curves and alpha diversity were determined using mothur v1.30.1 and beta diversity was determined using QIIME. Partial least squares discriminant analysis (PLS-DA) was achieved in R tools using package mixOmics. Data structure was analyzed by principal co-ordinates analysis (PCoA) using the Bray-Curtis dissimilarity

matrices. Linear discriminant analysis (LDA) coupled with effect size (LEfSe) was performed using LEfSe program.

Based on 16S rRNA gene sequence data, Tax4Fun, an open-source R package, was used to predict functional capacities of microbial communities mapping with Kyoto Encyclopedia of Genes and Genomes (KEGG) reference database.

2.6. Analysis of antioxidant capacity

In another set of study, male C57BL/6J mice (n = 6) were treated with *P. chinense* extract at a dosage of 0.4 g/kg via *p.o.* for 5 consecutive days. Control mice (n = 6) received vehicle. After treatment, mice were sacrificed after anaesthetization, and blood and liver tissues of each mouse were collected. Blood were further centrifuged at 4 ^{o}C at 4000 rpm/min for 5 min to obtain plasma. Fresh liver tissues were washed with cold PBS, and homogenized in normal saline at 4 ^{o}C. Protein contents of liver homogenate were determined using BCA Protein Assay kit (Beyotime Biotechnology, China) according to the manufacturer's instruction.

Plasma was used to determine superoxide dismutase (SOD) level. Total antioxidant capacity (T-AOC), catalase (CAT), glutathione (GSH) and glutathione peroxidase (GSH-Px) levels were determined using liver homogenate. All these parameters were analyzed using appropriate detection kits based on the manufacturer's instructions (Nanjing Jiancheng Bio-Engineering Institute Co.,Ltd, China).

2.7. Statistical analysis

Statistical difference was analyzed using GraphPad Prism software based on unpaired

student's *t* test (for comparison between two groups) or one-way ANOVA with a post hoc Bonferroni test (for comparison among three groups). All the results are considered statistically significant at $p < 0.05$.

3. Results and discussion

3.1. Identification of polyphenols in P. chinense

Based on LC-MS/MS, a total of 50 constituents were identified from the extract of *P. chinense* (Figure 1A and Table 1, *m/z* error < 5 ppm). Previous studies only reported 27 compounds using LC-MS/MS method (Guo et al., 2015). Among 50 identified compounds, 18 were confirmed with reference standards, while 32 were tentatively identified based on their accurate mass weight, fragmentations and comparison with previous reports, with 6 compounds (**39**, **41**, **42**, **44**, **45** and **49**) as potentially novel ones. All of them are (poly)phenols, including flavonoids, phenylpropanoids, phenolic acids and others. Polyphenols are important indigents of many plants (Zhao, Qiao, Shao, Hassan, Ma, & Yao, 2020). Their structures are displayed in Figure 2.

3.1.1. Flavonoids

Most flavonoids were identified as derivatives of pinocembrin, quercetin and kaempferol. Quercetin (**27**) eluting at 9.85 min showed a $[M+H]^+$ ion at *m/z* 303.0504 ($C_{21}H_{21}O_{11}$), which was identical with the reference standard. Compound **14** (Rt 9.32 min) yielded a $[M+H]^+$ at *m/z* 465.1041, producing a main fragment at *m/z* 303 ($C_{21}H_{21}O_{11}$) due to the loss of one glucose residue. It was confirmed with standard and

thus was identified as quercetin-3-*O*-glucoside. Compound **9** displaying a $[M+H]^+$ at *m/z* 627.1577 was characterized by successive loss of two glucose residues to produce fragments at *m/z* 465 and 303. It was identical to quercetin-di-*O*-glucoside (Guo et al., 2015). Both compounds **16** and **17** had a $[M+H]^+$ at *m/z* 435.0934 corresponding to $C_{20}H_{19}O_{11}$. The loss of 132 Da in their MS^2 spectra indicated the presence of a xylose or arabinose moiety. Based on previous reports (Wang, Jiang, Liu, Chen, Wu, & Zhang, 2014) or reference standard, compound **16** and **17** were quercetin-3-*O*-xyloside and quercetin-3-*O*-arabinfuranoside, respectively. Similarly, the characteristic fragment ion at *m/z* 303 in MS^2 spectra of **18** ($[M+H]^+$, *m/z* 449.1091), identical with reference standard, suggested that compound **18** was quercetin 3-*O*-rhamnoside.

Table 1. Identified compounds from *P. chinense* by UPLC-HR-MS.

No.	Identified compounds	Retention time (min)	Molecular formula ($[M+H]^+$)	$[M+H]^+$		MS^2 data (*m/z*)
				Detected (*m/z*)	Error (ppm)	
1	Chebulic acid*	1.43	$C_{14}H_{13}O_{11}$	357.04413	-3.102	339, 321, **293**, 275, 247, 203
2	Gallic acid*	2.41	$C_7H_7O_5$	171.0292	-0.925	153
3	Penthorumnin B	4.09	$C_{12}H_{11}O_8$	283.04389	-5.307	265, 237, 219, **191**
4	Ethyl gallate*	7.17	$C_9H_{11}O_5$	199.06059	2.462	181, **155**
5	Bergenin*	7.80	$C_{14}H_{17}O_9$	329.08734	1.919	**311**, 293, 275, 263, 247, 233, 221, 209, 197, 181, 133
6	Catechin*	8.03	$C_{15}H_{15}O_6$	291.0867	-0.457	273, 165, 147, **139**, 123
7	Brevifolin carboxylic acid*	8.03	$C_{13}H_9O_8$	293.02969	-0.178	275, 247, **219**, 205, 191, 177
8	Epicatechin*	8.56	$C_{15}H_{15}O_6$	291.08688	0.058	207, 165, 147, **139**, 123
9	Quercetin-di-*O*-glucoside	8.70	$C_{27}H_{31}O_{17}$	627.15771	3.403	465, **303**
10	Brevifolin	8.85	$C_{12}H_9O_6$	249.03860	-5.272	**207**, 193, 179
11	2,6-Dihydroxyacetophenone-4-O-glucoside	8.89	$C_{14}H_{19}O_9$	331.10291	1.665	**169**, 151
12	Penthorumin C	8.95	$C_{26}H_{25}O_{17}$	609.10788	-2.124	591, 439, **295**, 277
13	Rutin*	9.12	$C_{27}H_{31}O_{16}$	611.15972	-1.540	465, **303**, 129
14	Quercetin-3-*O*-glucoside*	9.32	$C_{21}H_{21}O_{12}$	465.10410	1.718	**303**, 229, 127
15	Kaempferol-3-*O*-rutinoside	9.47	$C_{27}H_{31}O_{15}$	595.16511	-1.070	449, **287**, 169

16	Quercetin-3-*O*-xyloside	9.52	$C_{20}H_{19}O_{11}$	435.09341	1.549	417, 345, **303**, 291, 167, 115
17	Quercetin-3-*O*-arabinfuranoside*	9.75	$C_{20}H_{19}O_{11}$	435.09357	1.916	399, **303**, 291, 115
18	Quercetin 3-*O*-rhamnoside*	9.85	$C_{21}H_{21}O_{11}$	449.10910	1.589	413, 345, **303**, 287, 273, 229, 129
19	Naringenin-7-*O*-glucoside	10.21	$C_{21}H_{23}O_{10}$	435.12962	1.145	417, 339, 303, **273**, 219, 153
20	Kaempferol-3-*O*-arabinfuranoside	10.42	$C_{20}H_{19}O_{10}$	419.09827	1.07	383, 353, **287**, 275, 247
21	Kaempferol-3-*O*-rhamnopyranoside	10.69	$C_{21}H_{21}O_{10}$	433.11401	1.243	397, 329, **287**, 211, 129
22	2,6-Dihydroxyacetophenone-4-*O*-[4',6'-hexahydroxydiphenoyl]-glucoside	10.90	$C_{28}H_{25}O_{17}$	633.10798	-1.886	615, 597, 465, 303, 277, 259, 211, **169**, 153
23	Pinostrobin	10.95	$C_{16}H_{15}O_4$	271.09701	-0.088	253, **167**, 131
24	2,3′-Dihydroxy-3-methoxy-6′-methanone-benzophenone-4-*O*-glucoside	11.83	$C_{25}H_{29}O_{11}$	505.16931	-3.319	487, 343, 325, **203**, 151, 127
25	2,4-Dihydroxy-3-methoxy-6′-methanone-benzo-phenone-3′-*O*-glucoside	12.07	$C_{25}H_{27}O_{11}$	505.16947	-3.002	487, 443, 343, 325, **203**, 127
26	Luteolin*	12.57	$C_{15}H_{11}O_6$	287.05545	-0.393	**269**, 153, 123, 107
27	Quercetin*	12.71	$C_{15}H_{11}O_7$	303.05038	-0.322	285, **257**, 229, 201, 165, 153, 137
28	Penthorumnin C	12.76	$C_{27}H_{25}O_{17}$	621.10760	-2.534	603, 585, 453, 393, 291, 277, 259, 211, **169**
29	Pinocembrin-7-*O*-glucoside	14.38	$C_{21}H_{23}O_9$	419.13484	1.510	383, **257**, 239, 153, 131
30	Apigenin*	15.05	$C_{15}H_{11}O_5$	271.06073	0.301	253, 229, 203, **153**

31	Pinocembrin-7-*O*-[3"-*O*-galloyl]-glucoside	15.05	$C_{28}H_{27}O_{13}$	571.14665	3.559	365, 297, 257, 219, 195, 171, **153**, 127
32	Isomer of Pinocembrin-7-*O*-[3"-*O*-galloyl]-glucoside	15.43	$C_{28}H_{27}O_{13}$	571.14657	3.419	515, 449, 401, 365, 297, 257, 195, 171, **153**, 127
33	Kaempferol*	15.72	$C_{15}H_{11}O_6$	287.05545	-0.393	269, 241, 213, 165, **153**, 121
34	Isomer of Pinocembrin-7-*O*-[3"-*O*-galloyl]-glucoside	16.24	$C_{28}H_{27}O_{13}$	571.14676	3.752	553, 451, 401, 365, 315, 299, 281, 269, 257, 219, 195, 177, **153**, 131
35	Isomer of Pinocembrin-7-*O*-[3"-*O*-galloyl]-glucoside	18.20	$C_{28}H_{27}O_{13}$	571.14682	3.857	571, 535, 365, 347, 299, 269, **257**, 195, 171, 153, 131
36	Isomer of Pinocembrin-7-*O*-[3"-*O*-galloyl]-glucoside	18.68	$C_{28}H_{27}O_{13}$	571.14687	3.944	535, 365, 335, 269, **257**, 171, 153, 131
37	2',4',6'-Trihydroxydihydrochalcone-4'-glucoside	19.04	$C_{21}H_{25}O_9$	421.14853	-3.151	337, 301, **259**, 241, 133, 105
38	Pinocembrin-7-*O*-[4",6"-hexahydroxydiphenoyl]-glucoside	20.15	$C_{35}H_{29}O_{17}$	721.13936	-1.545	637, 559, 465, 365, 303, 277, **257**, 243, 153, 131
39	2',6'-Dihydroxydihydrochalcone-4'-*O*-[3"-*O*-galloyl]-glucoside	20.24	$C_{28}H_{29}O_{13}$	573.15950	-2.295	315, 297, 259, 171, **153**, 127, 105
40	Penchinone A	20.83	$C_{19}H_{19}O_6$	343.11829	0.370	325, **203**, 175
41	Isomer of 2',6'-Dihydroxydihydrochalcone-4'-*O*-[3"-*O*-galloyl]-glucoside	20.91	$C_{28}H_{29}O_{13}$	573.15930	-2.644	537, 453, 367, 283, 259, **153**, 105
42	Pinocembrin-7-*O*-[3"-*O*-galloyl-4",6"-hexahydroxydiphenoyl]-glucoside isomer	21.87	$C_{42}H_{33}O_{21}$	873.15015	-1.469	855, 617, 517, 447, 365, 303, **257**, 171, 153, 127

43	Penchinone B	22.89	$C_{19}H_{19}O_6$	343.11832	0.457	325, **203**, 175
44	Isomer of 2',6'-Dihydroxydihydrochalcone-4'-*O*-[3"-*O*-galloyl]-glucoside	22.93	$C_{28}H_{27}O_{13}$	573.15980	-1.772	529, 477, 367, 349, 315, 271, **259**, 171, 153, 105
45	Isomer of 2',6'-Dihydroxydihydrochalcone-4'-*O*-[3"-*O*-galloyl]-glucoside	23.41	$C_{28}H_{27}O_{13}$	573.15992	-1.563	349, 337, **259**, 171, 153, 105
46	Pinocembrin-7-*O*-[3"-*O*-galloyl-4",6"-hexahydroxydiphenoyl]-glucoside*	24.22	$C_{42}H_{33}O_{21}$	873.15082	-0.702	855, 705, 617, 517, 365, 303, **257**, 171, 153, 127
47	Pinocembrin-dihydrochalcone-7-*O*-[4",6"-hexahydroxydiphenoyl]-glucoside	24.75	$C_{35}H_{31}O_{17}$	723.15794	-0.757	705, 687, 555, 465, 367, 349, 303, 277, **259,** 241, 127, 105
48	Pinocembrin*	25.47	$C_{15}H_{13}O_4$	257.08134	-0.170	239, 215, 173, **153**, 131
49	2-hydroxyacetophenone 4-*O*-[4',6'-hexahydroxydiphenoyl]-glucoside	26.12	$C_{27}H_{21}O_{17}$	617.07636	-1.565	599, 447, 303, 277, **153**, 127
50	Thonningianin A*	28.38	$C_{42}H_{35}O_{21}$	875.16956	0.130	857, 617, 555, 537, 447, 385, 367, 303, 277, **259**, 171, 153, 127, 105

***** Confirmed with reference standards.

Kaempferol (**33**, $C_{15}H_{10}O_6$) was observed at 15.72 min. Compounds **15**, **20** and **21** displayed molecular ions at *m/z* 595.1651, 419.0983 and 433.1140, respectively, which produced a common fragment at *m/z* 287 ($C_{15}H_{11}O_6$). The loss of 308, 132 and 146 Da corresponded to residues of rutinose, arabinose and rhamnose, respectively. Compound **15**, **20** and **21** were thus identified as kaempferol-3-*O*-rutinoside, kaempferol-3-*O*-arabinfuranoside and kaempferol-3-*O*-rhamnopyranoside, respectively. On this basis, compound **15** was further confirmed with reference standard.

Pinocembrin (**48**) along with other 14 derivatives (**23**, **29**, **31**, **32**, **34**-**36**, **38**, **39**, **41**, **42**, **44**, **45**-**47**, **50**) were identified. Pinocembrin eluted at 25.47 min with $[M+H]^+$ at *m/z* 255.0660 and was identical with reference standard. Compound **23** was identified as pinostrobin, showing $[M+H]^+$ at 271.09701 ($C_{16}H_{15}O_4$). The key fragment at *m/z* 167 suggested that an *O*-methyl group in A ring. Compound **29** was identified as pinocembrin-7-*O*-glucoside, due to the characteristic loss of 162 Da ($C_6H_{10}O_5$) corresponding to a glucose residue (He et al., 2015). Compound **31**, **32**, **34**-**36** showed a molecular ion at *m/z* 571.1468 ($[M+H]^+$, $C_{28}H_{27}O_{13}$). The presence of a key fragment at *m/z* 257 ($C_{15}H_{13}O_4$) indicated that they are pinocembrin derivatives. The characteristic loss of 314 Da from the ion *m/z* 571 and the presence of a fragment at *m/z* 153 ($C_7H_5O_4$) suggested a galloyl-glucose residue in their structures. These five compounds were thus identified as pinocembrin-7-*O*-galloyl-glucoside and isomers (Guo et al., 2015). Compounds **38** and **47** were identified as pinocembrin-7-*O*-[4",6"-hexahydroxydiphenoyl]-glucoside and pinocembrin-dihydrochalcone-7-*O*-[4",6"-

hexahydroxydiphenoyl]-glucoside, respectively, which had $[M+H]^+$ at *m/z* 721.1394 ($C_{35}H_{29}O_{17}$) and 723.1579 ($C_{35}H_{31}O_{17}$) (Guo, et al., 2015). The presence of fragments at *m/z* 303 and 257 for **38** and ions at *m/z* 303 and 259 for **47** indicated the loss of a glucose moiety and a hexahydroxydiphenoyl residue. The fragment at *m/z* 153 was an indicator of the galloyl moiety. Similarly, **46** and **50** showing $[M+H]^+$ at *m/z* 873.1502 and 875.1696 were characterized as pinocembrin-7-*O*-[3"-*O*-galloyl-4",6"-hexahydroxydiphenoyl]-glucoside and thonningianin A, which were confirmed with reference standards. They presented characteristic ions at *m/z* 303, 257, 153 for **46** and *m/z* 303, 259, 153 for **50**. Compound **42** having similar fragmentations with **46** was identified as an isomer of **46**. Compound **39** showed $[M+H]^+$ at *m/z* 573.15950 ($C_{28}H_{29}O_{13}$) with key fragment ions at *m/z* 259, 153 and 105. It was identified as 2',6'-dihydroxydihydrochalcone-4'-*O*-[3"-*O*-galloyl]-glucoside. Three isomers (**41**, **44** and **45**) of **39** were found at 20.91, 22.93 and 23.41 min, respectively. They shared similar fragmentation pathways.

Other flavonoids included **4** (ethyl gallate), **6** (catechin), **8** (epicatechin), **13** (rutin), **19** (naringenin-7-*O*-glucoside), **26** (luteolin) and **30** (apigenin). The retention time, MS and MS^2 data of **6**, **8**, **13**, **26** and **30** were identical with the reference standards. Compound **19** eluting at 10.21 min had a $[M+H]^+$ at *m/z* 435.12962 ($C_{21}H_{23}O_{10}$) . The loss of a glucose residue resulted in the presence of a key fragment at *m/z* 273.

Taken together, a total of 34 flavonoids were identified. Among them, compound **39**, **41**, **42**, **44** and **45** were reported for the first time.

3.1.2. Phenylpropanoids

A total of four phenylpropanoids (**24**, **25**, **40** and **43**) were found in *P. chinense*. Both **24** and **25** displayed $[M+H]^+$ at *m/z* 505.16931 with calculated molecular formula of $C_{25}H_{29}O_{11}$. They shared similar fragments such as ions at *m/z* 487 ($C_{25}H_{27}O_{10}$, $[M+H-H_2O]^+$), 343 ($C_{19}H_{19}O_6$, [M+H-glucose residue]$^+$), 325 ($C_{19}H_{17}O_5$, [M+H-H_2O-glucose residue]$^+$) and 203 ($C_{12}H_{11}O_3$). Based on previous report (Huang, Wang, Sun, Chen, & Sun, 2018), **24** and **25** were 2,3′-dihydroxy-3-methoxy-6′-methanone-benzophenone-4-*O*-glucoside and 2,4-dihydroxy-3-methoxy-6′-methanone-benzo-phenone-3′-*O*-glucoside, respectively. Compound **40** and **43** ($[M+H]^+$, *m/z* 343.1183; $C_{19}H_{19}O_6$) had key fragments at *m/z* 325 and 203. They were identified as penchinone A and penchinone B, respectively (He et al., 2015).

3.1.3. Others

Several other phenolic compounds (**1**-**3**, **5**, **7**, **10**-**12**, **22**, **28**, **37** and **49**) were also identified, with **2**, **5** and **7** confirmed with standards. Compound **1** was detected at 1.43 min with calculated formula of $C_{14}H_{13}O_{11}$. Its characteristic fragments included ions at *m/z* 339 ($C_{14}H_{11}O_{10}$, $[M+H-H_2O]^+$), 321 ($C_{14}H_9O_9$, $[M+H-2H_2O]^+$), 293 ($C_{13}H_{11}O_9$, $[M+H-H_2O-HCOOH]^+$), 275 ($C_{13}H_9O_8$, $[M+H-2H_2O-HCOOH]^+$), and 247 ($C_{12}H_9O_7$, $[M+H-H_2O-2HCOOH]^+$), which was identical with chebulic acid. Compound **3** ($[M+H]^+$, *m/z* 283.0439) underwent successive loss of HCOOH (46 Da) and H_2O, and was identified as penthorumnin B (Era, Matsuo, Saito, Nishida, Jiang, & Tanaka, 2018). Compound **11** ($[M+H]^+$, $C_{14}H_{19}O_9$) had a characteristic fragment ion at *m/z* 169,

indicating the loss of a glucose residue. It is identified as 2,6-dihydroxyacetophenone-4-*O*-glucoside (Sun et al., 2018). Compound **12** was identified as penthorumin C, showing main fragmentations at *m/z* 591 ($[M+H-H_2O]^+$), 439 ($[M+H-C_7H_8O_5]^+$), and 295 ($[M+H-C_{14}H_{13}O_9]^+$) (Huang, Jiang, Chen, Yao, & Sun, 2014). Compound **22** was detected at 10.90 min with $[M+H]^+$ at *m/z* 633.1080. The key fragments at *m/z* 303 and 153 suggested the presence of a hexahydroxydiphenoyl-glucose residue. The fragment ion at *m/z* 169 was identical with the residue of 2,4,6-trihydroxyacetophenone. It was identified as 2,6-dihydroxyacetophenone-4-*O*-[4',6'-hexahydroxydiphenoyl]-glucoside (Huang, Jiang, Chen, Yao, & Sun, 2014). Compound **28** was penthorumnin C, which showed characteristic ions at *m/z* 453 ($C_{19}H_{17}O_{13}$), 291 ($C_{13}H_7O_8$) and 169 ($C_8H_9O_4$) (Era, Matsuo, Saito, Nishida, Jiang, & Tanaka, 2018). Compound **37** eluting at 19.04 min displayed $[M+H]^+$ at *m/z* 421.1485, with main fragmentations at *m/z* 259, 133 and 105. Fragment at *m/z* 259 was due to the loss of a glucose residue, and *m/z* 133 and 105 corresponded to phenemyl and phenylacetyl groups, respectively. It was identified as 2',4',6'-trihydroxydihydrochalcone-4'-glucoside (Sun et al., 2018). Compound **49** was identified as an analogue of compound **11** and **22**, which had a dominant characteristic fragment at *m/z* 153 (a 2,4,6-trihydroxyacetophenone residue). The presence of ions at *m/z* 303 and 153 indicated a hexahydroxydiphenoyl-glucose group. It was thus identified as 2-hydroxyacetophenone 4-*O*-[4',6'-hexahydroxydiphenoyl]-glucoside (Huang, Jiang, Chen, Yao, & Sun, 2014). Compound **49** was reported for the first time. The proposed fragmentation is shown in Figure 1B.

In summary, almost all identified compounds here are polyphenols. Some of them such as thonningianin A, thonningianin B, pinocembrin, pinocembrin-7-*O*-[3"-*O*-galloyl-4",6"-hexahydroxydiphenoyl]-glucoside, pinocembrin-7-*O*-glucoside and quercetin have been reported to possess remarkable antioxidant and anti-inflammatory effect and protect mice from liver injury induced by high-fat diet, alcohol or other chemicals (Sun et al., 2018). These polyphenols might be the most important active principals of *P. chinense* for alleviating liver diseases.

3.2. Total flavonoid and phenolic contents of P. chinense

Since polyphenols are identified as the main constituents of *P. chinense*, we further quantified the total flavonoid and phenolic contents. The results (Figure 1C) showed that the total flavonoid content of *P. chinense* was 465.6 ± 34.4 mg RE/g (46.6%, *w/w*), and the total phenolic content was 612.9 ± 45 mg GAE/g (61.3%, *w/w*), suggesting that *P. chinense* extract are enriched with polyphenols.

3.3. Determination of individual phenolic compounds in P. chinense

Since different pretreatment methods may significantly affect quality and chemical composition of herbal extract, here we performed LC-MS-based quantification on *P. chinense* extract to ensure its quality (Hassan, Umar, Ding, Mehryar, & Zhao, 2017; Zhao, Cao, Ma, & Shao, 2017; Qiao, Zhao, Shao, & Hassan, 2018; Zhang et al., 2019). We further determined the amounts of 13 polyphenols, including **7**, **13**, **14**, **15**, **17**, **18**, **26**, **27**, **29**, **30**, **37**, **46**, and **50**, in *P. chinense* extract using LC-QqQ-MS/MS. All these compounds have been reported to have remarkable bioactivities either *in vitro* or *in vivo*.

The results (Figure 1D) indicated that among all detected constituents the compound **29** (Pinocembrin 7-*O*-glucoside) accounted for the highest contents (250.8 ± 13.4 mg/g), followed by compound **50** (52.2 ± 8.4 mg/g) and **7** (14.9 ± 1.2 mg/g). The contents of compounds **18**, **27** and **46** were 5.75 ± 0.98, 1.18 ± 0.1 and 6.02 ± 0.64 mg/g, respectively. The amounts of other compounds were all below 1 mg/g. The total contents of all detected compounds accounted for 33.1% (*w/w*) of *P. chinense* extract. It is suggested that polyphenols are major chemical constituents of *P. chinense*.

3.4. Modulation of gut microbiota by P. chinense

P. chinense and its preparations have been widely used for treatment of several liver diseases, however, with undefined mechanism of actions. Previous studies have shown that alteration of gut microbiota compositions is closely associated with occurrence and progression of non-alcoholic and alcoholic fatty liver disease (NAFLD and AFLD), cirrhosis as well as hepatocellular carcinoma (Schnabl & Brenner, 2014). Disruption of the microbial homeostasis is often known as dysbiosis, which is tightly modulated by both environmental (*e.g.*, diet, exposure to chemicals or antibiotics, hygiene, *etc*.) and genetic factors and a specialized mucosa-host immune system (Brandl et al., 2008). Intestinal microbiota has a profound impact on liver diseases via several ways. Many researches have thus highlighted the use of probiotics and prebiotics as new therapeutic strategies for liver diseases and other metabolic syndrome.

Recent studies found that natural polyphenols or polyphenol-rich diet may be potential prebiotics to regulate compositions of gut microbiota (Selma, Espin, & Tomasbarberan,

2009). For instance, tea polyphenol intake (0.4 g, 3 times daily for 4 weeks) led to increased growth of *Clostridium* species and decreased level of *Bifidobacterium* (Okubo et al., 1992). Although polyphenols are usually of low bioavailability, they may have a direct impact on intestinal microbiota. Since polyphenols are identified as main constituents of *P. chinense*, we hypothesize that *P. chinense* may be a prebiotic herb *in vivo*. To see whether and how *P. chinense* shapes gut microbiota composition, we performed 16S rRNA gene sequencing with mice feces collected before and after daily oral administration of *P. chinense* extract (at 0.4 g/kg for 5 days). The dose used for mice is generally equivalent to that used in human after a compensation for species difference. The experimental design is shown in Figure 3A.

As shown in Figure 3B and 3C, after a 5-day ingestion of *P. chinense*, the richness of microbiota reflected as Sobs index had a minimal change, while the diversity of microbial community indicated by Shannon index was significantly elevated ($p < 0.05$). The result also showed that the *P. chinense*-induced changes in α diversity (Indicated by Shannon index) were recovered after one week of drug-free wash. As displayed in supplementary Figure 1 by rarefaction curves, the curves became much flatter to the right, suggesting that sufficient numbers of sequences were obtained and the α diversity of the sampled community was reasonably calculated.

Moreover, a structural rearrangement of gut microbiota was observed after *P. chinense* treatment as displayed by a supervised PLS-DA and PCoA (Figure 3D and 3E). The *P. chinense*-treated group was quite different from the control group, while after 1 week

of recovery they showed increased similarities with the control group. At phylum level, with the treatment of *P. chinense* extract, the abundance of *Firmicutes*, *Actinobacteria*, and *Deferribacteres* were decreased, while that of *Bacteroidetes*, *Proteobacteria*, *Cyanobacteria*, and *Verrucomicrobia* were increased (Figure 3F). In previous reports, the predominance of *Firmicutes* and decreased level of *Bacteroidetes* was positively associated with obesity, irritable bowel syndrome, and non-alcoholic steatohepatitis (NASH) (Boursier & Diehl, 2015). Here, *P. chinense*-induced change regarding decreased ratio of *Firmicutes*/*Bacteroidetes* (from 1.08% to 0.82%) might be a beneficial factor against dysbiosis.

The *P. chinense*-induced alteration in microbiota composition is displayed in Figure 4C (Bacterial taxonomic profiling at the genus level of gut bacteria). The heatmap showed the mean abundance of 50 main genus which were significantly altered. We also performed LEfSe analysis and identified a group of bacteria that were remarkably different among groups (Figure 4A and 4B). Generic differences are displayed in Figure 4D. After *P. chinense* treatment for 5 days, the abundance of genus *norank_f_Muribaculaceae* was significantly decreased from 42.4% to 20.4% ($p < 0.05$), while that of *Rikenellaceae_RC9_gut_group*, *Prevotellaceae_UCG-001*, *Bacteroides*, *Akkermansia*, *Ruminiclostridium*, *Ruminococcaceae_UCG-010*, *Ruminococcaceae_NK4A214_group*, *norank_Ruminococcaceae*, and *Ruminococcaceae_UCG-009* were significantly increased ($p < 0.05$). Compared to

control group, these changes in *P. chinense*-treated group became recovered, at least partially, after a 1-week drug-free wash.

The family *Muribaculaceae*, previously known as *S24-7*, has been reported to involve in complex carbohydrate degradation (Lagkouvardos et al., 2019). Several studies have indicated a correlation of alteration of *Muribaculaceae* with high-fat diet, NAFLD and experimental colitis (Brenner, Paik, & Schnabl, 2015). Enriched *Muribaculaceae* has been reported in diabetes-sensitive mice fed with a high-fat diet (Serino et al., 2012), as well as in mice with remission of colitis (Rooks et al., 2014), although its role in progression of these pathological processes is still unclear. The genus *Bacteroides* contains several potential pathogenic species such as *B. fragilis* and *B. thetaiotaomicron* as well as some beneficial bacteria (*e.g.*, *B. acidifaciens*) (Wexler, 2007). It is found that *B. acidifaciens* prevented obesity and improved insulin sensitivity in mice (Yang et al., 2017). With a closer look, after *P. chinense* treatment, the abundance of *B. acidifaciens* and *B. sartorii* were increased (supplementary Figure 2). The exact role of *Prevotellaceae_UCG-001 (*family *Prevotellaceae)* in health has not been recognized. One study showed that *Prevotellaceae_UCG-001* was upregulated upon inulin treatment in *ob/ob* mice and was negatively correlated with markers of glycolipid metabolism disorders (Song et al., 2019). In rats with acute necrotizing pancreatitis, *Prevotellaceae_UCG-001* level was decreased (Chen et al., 2017). *Rikenellaceae_RC9_gut_group* (in family *Bacteroidetes*) has an impact on polysaccharides which may promote short-chain fatty acids (SCFAs) synthesis (Liu et

al., 2017). A recent study showed that *Rikenellaceae_RC9_gut_group* was enriched upon treatment of dietary fiber (Tao et al., 2019). *Akkermansia* belongs to *Verrucomicrobia* family. Low levels of *Akkermansia* are associated with a variety of conditions, such as Crohn's Disease, diabetes, and obesity (Derrien, Belzer, & De Vos, 2017). *Akkermansia* bacteria (*e.g.*, *A. muciniphila*) are known to be beneficial for intestinal health and glucose homeostasis (Derrien, Belzer, & De Vos, 2017). *Ruminiclostridium, Ruminococcaceae_UCG-010*, *Ruminococcaceae_NK4A214_group*, *norank_Ruminococcaceae*, and *Ruminococcaceae_UCG-009* belong to the family *Ruminococcaceae*. The abundance of *Ruminococcaceae* is significantly and positively correlated with increased intestinal permeability (Leclercq et al., 2014). *Ruminococcaceae* bacteria are known to have a beneficial effect on gut barrier function (Madsen et al., 2001). Taken together, *P. chinense*-induced alteration of gut microbiota composition might contribute to the liver protection benefit of *P. chinense*.

Interestingly, the genus *Alistipes* and *Odoribacter* had a minimal increase after *P. chinense* treatment, however, their levels were increased significantly after 1 week post treatment (Figure 4B). Abundance of *Alistipes* has been reported to be decreased in patients with inflammatory bowel disease including ulcerative colitis and Crohn's disease (Dalal & Chang, 2014). A study showed a positive association between *Alistipes* bacteria and improvement of DSS-induced colitis (Walker et al., 2017). Both *Alistipes* and *Odoribacter* are known producer of acetate, propionate, butyrate (Göker

et al., 2011), and sphingolipids (Walker et al., 2017), which are important for maturation of intestine or immune system as well as regulation of host inflammation.

Putting the above pieces together, *P. chinense* alters compositions of gut microbiota in mice. Notably, the shifted gut microbiota is toward an increased abundance of some beneficially anti-inflammatory and gut health-promoting bacteria.

3.5. Metabolic features of the resulting bacterial communities

To see how the altered structure of the gut microbiota impacted its metabolic potential, we further profiled the 16S rRNA sequencing data using Tax4Fun to predict the likely functional changes within biochemical pathways. The results showed that *P. chinense* treatment significantly enriched genes encoding KEGG metabolic pathways involved in metabolism (Figure 4E). Specifically, the main altered metabolic pathways (with abundance > 1%) included ko00051 (fructose and mannose metabolism), ko00240 (pyrimidine metabolism), ko00260 (glycine, serine and threonine metabolism), ko00300 (lysine biosynthesis), ko00550 (peptidoglycan biosynthesis), ko00564 (glycerophospholipid metabolism), and ko00900 (terpenoid backbone biosynthesis) (Figure 4F). It is suggested that *P. chinense* administration may have an impact on metabolism of carbohydrate, nucleotide, amino acid, lipid as well as terpenoids. In addition, the two-component system pathway (ko02020 relating with environmental information processing) was also enriched (Figure 4F), suggesting an enhanced ability of bacteria to sense, respond and adapt to environmental changes. Collectively,

functional shift of the gut microbiota by *P. chinense* treatment was toward an environment that is not easily susceptible to metabolic stress.

3.6. Antioxidant Activity

Oxidative stress plays an important role in development of metabolic syndromes such as obesity, liver steatosis, diabetes and hypertension, which is often associated with a dysregulation of redox balance (Cichoż-Lach & Michalak, 2014). We thus subsequently analyzed the activity of several antioxidant enzymes in systems after *P. chinense* treatment in mice (Figure 5). It is shown that *P. chinense* treatment significantly enhanced plasma SOD activity ($p < 0.05$; 166.6 ± 20.1 *vs* 130.7 ± 6.6 U/mL, *P. chinense* group vs control group) (Figure 5A). Moreover, the total antioxidant capacity (Figure 5B) as well as the activities of CAT (Figure 5C) and GSH-Px (Figure 5D) in mouse liver were significantly increased after treatment of *P. chinense*. The GSH level in mouse liver showed a trend of increase but with no statistical significance (Figure 5E). The results suggest that *P. chinense* promoted antioxidant activity in mice. Alteration of gut microbiota might have contributed to the beneficial effect of *P. chinense*.

4. Conclusion

Taken all the above results together, we identified 50 phenolic constituents from *P. chinense* based on UPLC-HR-MS, with 6 of them potentially novel ones. Total flavonoid and phenolic contents of *P. chinense* were 465.6 ± 34.4 mg RE/g and 612.9 ± 45 mg GAE/g, respectively. Further determination of 13 polyphenols in *P. chinense*

revealed that all detected compounds accounted for 33.1% (*w/w*) of *P. chinense*. It is suggested that *P. chinense* is enriched with polyphenols.

Notably, a 5-day treatment of *P. chinense* significantly altered composition of gut microbiota in mice toward a beneficially anti-inflammatory and gut health-promoting environment. Gut microbiota was characterized by decreased *norank_f_Muribaculaceae*, and increased level of *Rikenellaceae_RC9_gut_group*, *Prevotellaceae_UCG-001*, *Bacteroides*, *Akkermansia*, *Ruminiclostridium*, *Ruminococcaceae_UCG-010*, *Ruminococcaceae_NK4A214_group*, *norank_Ruminococcaceae*, and *Ruminococcaceae_UCG-009*. We further demonstrated that *P. chinense* enhanced antioxidant activity in mice, showing a potential prebiotic effect. This study provides a new mechanism insight into the health promoting effect of *P. chinense* and the potential protective role in fighting metabolic diseases.

Conflict of interest

The authors declare no competing financial interest.

Acknowledgement

This work was supported by the National Natural Science Foundation of China (No. 81703807), the Science and Technology Development Fund, Macao SAR (No. 0023/2019/A), National Key Research and Development Program of China (No.

2017YFE0191500), and grants from the Sichuan Science and Technology Program (No. 2019YJ0485) and the Joint Funds of the Southwest Medical University & Luzhou (NO. 2018LZXNYD-ZK34).

References

Bose, M., Lambert, J. D., Ju, J., Reuhl, K. R., Shapses, S. A., & Yang, C. S. (2008). The Major Green Tea Polyphenol, (-)-Epigallocatechin-3-Gallate, Inhibits Obesity, Metabolic Syndrome, and Fatty Liver Disease in High-Fat–Fed Mice. *Journal of Nutrition, 138*(9), 1677-1683.

Boursier, J., & Diehl, A. M. (2015). Implication of gut microbiota in nonalcoholic fatty liver disease. *PLoS Pathog, 11*(1), e1004559.

Brandl, K., Plitas, G., Mihu, C. N., Ubeda, C., Jia, T., Fleisher, M., Schnabl, B., DeMatteo, R. P., & Pamer, E. G. (2008). Vancomycin-resistant enterococci exploit antibiotic-induced innate immune deficits. *Nature, 455*(7214), 804-807.

Brenner, D. A., Paik, Y. H., & Schnabl, B. (2015). Role of Gut Microbiota in Liver Disease. *Journal of Clinical Gastroenterology, 49*(Suppl 1), S25-S27.

Carding, S., Verbeke, K., Vipond, D. T., Corfe, B. M., & Owen, L. J. (2015). Dysbiosis of the gut microbiota in disease. *Microbial ecology in health and disease, 26*, 26191-26191.

Chen, J., Huang, C., Wang, J., Zhou, H., Lu, Y., Lou, L., Zheng, J., Tian, L., Wang, X., Cao, Z., & Zeng, Y. (2017). Dysbiosis of intestinal microbiota and decrease in paneth cell antimicrobial peptide level during acute necrotizing pancreatitis in rats. *Plos One, 12*(4), e0176583.

Cichoż-Lach, H., & Michalak, A. (2014). Oxidative stress as a crucial factor in liver diseases. *World J. Gastroenterol., 20*(25), 8082.

Dalal, S. R., & Chang, E. B. (2014). The microbial basis of inflammatory bowel diseases. *The Journal of clinical investigation, 124*(10), 4190-4196.

Derrien, M., Belzer, C., & De Vos, W. M. (2017). Akkermansia muciniphila and its role in regulating host functions. *Microbial Pathogenesis, 106*, 171-181.

Era, M., Matsuo, Y., Saito, Y., Nishida, K., Jiang, Z.-H., & Tanaka, T. (2018). Ellagitannins and Related Compounds from Penthorum chinense. *Journal of Natural Products*, *82*(1):129-135.

Göker, M., Gronow, S., Zeytun, A., Nolan, M., Lucas, S., Lapidus, A., Hammon, N., Deshpande, S., Cheng, J.-F., Pitluck, S., Liolios, K., Pagani, I., Ivanova, N., Mavromatis, K.,

Ovchinikova, G., Pati, A., Tapia, R., Han, C., Goodwin, L., Chen, A., Palaniappan, K., Land, M., Hauser, L., Jeffries, C. D., Brambilla, E.-M., Rohde, M., Detter, J. C., Woyke, T., Bristow, J., Markowitz, V., Hugenholtz, P., Eisen, J. A., Kyrpides, N. C., & Klenk, H.-P. (2011). Complete genome sequence of Odoribacter splanchnicus type strain (1651/6). *Standards in genomic sciences, 4*(2), 200-209.

Guinane, C. M., & Cotter, P. D. (2013). Role of the gut microbiota in health and chronic gastrointestinal disease: understanding a hidden metabolic organ. *Therapeutic advances in gastroenterology, 6*(4), 295-308.

Guo, W., Jiang, Y., Chen, X., Yu, P., Wang, M., Wu, X., & Zhang, D. (2015). Identification and quantitation of major phenolic compounds from penthorum chinense pursh. by HPLC with tandem mass spectrometry and HPLC with diode array detection. *Journal of Separation Science, 38*(16), 2789-2796.

He, Y.-C., Peng, C., Xie, X.-F., Chen, M.-H., Li, X.-N., Li, M.-T., Zhou, Q.-M., Guo, L., & Xiong, L. (2015). Penchinones A–D, two pairs of cis-trans isomers with rearranged neolignane carbon skeletons from Penthorum chinense. *RSC Advances, 5*(94), 76788-76794.

Hassan, M., Umar, M., Ding, W., Mehryar, E., Zhao, C. (2017). Methane enhancement through co-digestion of chicken manure and oxidative cleaved wheat straw: Stability performance and kinetic modeling perspectives. *Energy*, *141*, 2314-2320.

Huang, D., Jiang, Y., Chen, W., Yao, F., & Sun, L. (2014). Polyphenols with anti-proliferative activities from Penthorum chinense Pursh. *Molecules, 19*(8), 11045-11055.

Huang, D., Wang, X., Sun, L., Chen, W., & Sun, L. (2018). Two new phenylpropanoids from Penthorum chinense Pursh. *Phytochemistry Letters, 28*, 84-87.

Lagkouvardos, I., Lesker, T. R., Hitch, T. C. A., Gálvez, E. J. C., Smit, N., Neuhaus, K., Wang, J., Baines, J. F., Abt, B., Stecher, B., Overmann, J., Strowig, T., & Clavel, T. (2019). Sequence and cultivation study of Muribaculaceae reveals novel species, host preference, and functional potential of this yet undescribed family. *Microbiome, 7*(1), 28.

Leclercq, S., Matamoros, S., Cani, P. D., Neyrinck, A. M., Jamar, F., Stärkel, P., Windey, K., Tremaroli, V., Bäckhed, F., Verbeke, K., de Timary, P., & Delzenne, N. M. (2014). Intestinal permeability, gut-bacterial dysbiosis, and behavioral markers of alcohol-dependence severity. *Proceedings of the National Academy of Sciences of the United States of America, 111*(42), E4485-E4493.

Liu, P., Zhao, J., Guo, P., Lu, W., Geng, Z., Levesque, C. L., Johnston, L. J., Wang, C., Liu, L., Zhang, J., Ma, N., Qiao, S., & Ma, X. (2017). Dietary Corn Bran Fermented by Bacillus subtilis MA139 Decreased Gut Cellulolytic Bacteria and Microbiota Diversity in Finishing Pigs. *Front Cell Infect Microbiol, 7*, 526.

Madsen, K., Cornish, A., Soper, P., McKaigney, C., Jijon, H., Yachimec, C., Doyle, J., Jewell, L., & De Simone, C. (2001). Probiotic bacteria enhance murine and human intestinal epithelial barrier function. *Gastroenterology, 121*(3), 580-591.

Okubo, T., Ishihara, N., Oura, A., Serit, M., Kim, M., Yamamoto, T., & Mitsuoka, T. (1992). In Vivo Effects of Tea Polyphenol Intake on Human Intestinal Microflora and Metabolism. *Biosci Biotechnol Biochem, 56*(4), 588-591.

Orsavová, J., Hlaváčová, I., Mlček, J., Snopek, L., & Mišurcová, L. (2019). Contribution of phenolic compounds, ascorbic acid and vitamin E to antioxidant activity of currant (Ribes L.) and gooseberry (Ribes uva-crispa L.) fruits. *Food Chemistry, 284*, 323-333.

Qiao, X., Zhao, C., Shao, Q., & Hassan, M. (2018). Structural characterization of corn stover lignin after hydrogen peroxide presoaking prior to ammonia fiber expansion pretreatment. *Energy & Fuels*, *32*(5), 6022-6030.

Rooks, M. G., Veiga, P., Wardwell-Scott, L. H., Tickle, T., Segata, N., Michaud, M., Gallini, C. A., Beal, C., van Hylckama-Vlieg, J. E. T., Ballal, S. A., Morgan, X. C., Glickman, J. N., Gevers, D., Huttenhower, C., & Garrett, W. S. (2014). Gut microbiome composition and function in experimental colitis during active disease and treatment-induced remission. *The ISME journal, 8*(7), 1403-1417.

Schnabl, B., & Brenner, D. A. (2014). Interactions Between the Intestinal Microbiome and Liver Diseases. *Gastroenterology, 146*(6), 1513-1524.

Selma, M. V., Espin, J. C., & Tomasbarberan, F. A. (2009). Interaction between Phenolics and Gut Microbiota: Role in Human Health. *Journal of Agricultural and Food Chemistry, 57*(15), 6485-6501.

Serino, M., Luche, E., Gres, S., Baylac, A., Berge, M., Cenac, C., Waget, A., Klopp, P., Iacovoni, J., Klopp, C., Mariette, J., Bouchez, O., Lluch, J., Ouarne, F., Monsan, P., Valet, P., Roques, C., Amar, J., Bouloumie, A., Theodorou, V., & Burcelin, R. (2012). Metabolic adaptation to a high-fat diet is associated with a change in the gut microbiota. *Gut, 61*(4), 543-553.

Song, X., Zhong, L., Lyu, N., Liu, F., Li, B., Hao, Y., Xue, Y., Li, J., Feng, Y., Ma, Y., Hu, Y., & Zhu, B. (2019). Inulin Can Alleviate Metabolism Disorders in ob/ob Mice by Partially Restoring Leptin-related Pathways Mediated by Gut Microbiota. *Genomics, Proteomics & Bioinformatics, 17*(1), 64-75.

Sun, Z. L., Zhang, Y. Z., Zhang, F., Zhang, J. W., Zheng, G. C., Tan, L., Wang, C. Z., Zhou, L. D., Zhang, Q. H., & Yuan, C. S. (2018). Quality assessment of Penthorum chinense Pursh through multicomponent qualification and fingerprint, chemometric, and antihepatocarcinoma analyses. *Food Funct, 9*(7), 3807-3814.

Tao, S., Bai, Y., Zhou, X., Zhao, J., Yang, H., Zhang, S., & Wang, J. (2019). In Vitro Fermentation Characteristics for Different Ratios of Soluble to Insoluble Dietary Fiber by Fresh Fecal Microbiota from Growing Pigs. *ACS Omega, 4*(12), 15158-15167.

Walker, A., Pfitzner, B., Harir, M., Schaubeck, M., Calasan, J., Heinzmann, S. S., Turaev, D., Rattei, T., Endesfelder, D., Castell, W. z., Haller, D., Schmid, M., Hartmann, A., & Schmitt-Kopplin, P. (2017). Sulfonolipids as novel metabolite markers of Alistipes and Odoribacter affected by high-fat diets. *Scientific Reports, 7*(1), 11047.

Wang, A., Li, M., Huang, H., Xiao, Z., Shen, J., Zhao, Y., Yin, J., Kaboli, P.J., Cao, J., Cho, C.H., Wang, Y., Li, J., & Wu, X. (2020). A review of Penthorum chinense Pursh for hepatoprotection: Traditional use, phytochemistry, pharmacology, toxicology and clinical trials. *Journal of Ethnopharmacology*, *251*, 112569.

Wang, A., Wang, S., Jiang, Y., Chen, M., Wang, Y., & Lin, L. (2016). Bio-assay guided identification of hepatoprotective polyphenols from Penthorum chinense Pursh on t-BHP induced oxidative stress injured L02 cells. *Food & Function, 7*(4), 2074-2083.

Wang, M., Jiang, Y., Liu, H. L., Chen, X. Q., Wu, X., & Zhang, D. Y. (2014). A new flavanone from the aerial parts of Penthorum chinense. *Nat Prod Res, 28*(2), 70-73.

Wexler, H. M. (2007). Bacteroides: the good, the bad, and the nitty-gritty. *Clinical microbiology reviews, 20*(4), 593-621.

Yang, J. Y., Lee, Y. S., Kim, Y., Lee, S. H., Ryu, S., Fukuda, S., Hase, K., Yang, C. S., Lim, H. S., Kim, M. S., Kim, H. M., Ahn, S. H., Kwon, B. E., Ko, H. J., & Kweon, M. N. (2017). Gut commensal Bacteroides acidifaciens prevents obesity and improves insulin sensitivity in mice. *Mucosal Immunol, 10*(1), 104-116.

Zhang, M., Zhao, C., Chao Zhao, Shao, Q., Yang, Z., Zhang, X., Xu, X., & Hassan, M. (2019). Determination of water content in corn stover silage using near-infrared spectroscopy. *International Journal of Agricultural and Biological Engineering*, *12*(6), 143-148.

Zhao, C., Cao, Y., Ma, Z., & Shao, Q. (2017). Optimization of liquid ammonia pretreatment conditions for maximizing sugar release from giant reed (Arundo donax L.). *Biomass and Bioenergy*, *98*, 61-69.

Zhao, C., Qiao, X., Shao, Q., Hassan, M., Ma, Z., Yao, L. (2020). Synergistic effect of hydrogen peroxide and ammonia on lignin. *Industrial Crops and Products*, *146*, 112177.

Table legend

Table 1. Identified compounds from *P. chinense* by UPLC-HR-MS.

Figure captions

Figure 1. (A) Base-peak UPLC-HR-MS chromatogram of *P. chinense* extract annotated with identified constituents (**1-50**). (B) Fragmentation of compound **49** based on MS/MS spectrum. (C) Total flavonoid and phenolic contents of *P. Chinense* extract.

(D) Quantitative results of 13 polyphenols (**7**, **13**, **14**, **15**, **17**, **18**, **26**, **27**, **29**, **30**, **37**, **46**, and **50**) in *P. Chinense* extract.

Figure 2. The structure of identified polyphenols from *P. chinense* extract. HHDP, hexahydroxydiphenoyl; glu, glucose; rha, rhamnose; xyl, xylose; ara, arabinfuranose.

Figure 3. Structural modulation of gut microbiota by *P. chinense* in mice. (A) Schematic illustration of experimental procedures. Male C57BL/6J mice were adapted in SPF-grade animal house for two weeks before conducting experiment. Mice were orally given PE at 0.4 g/kg once daily (at 9:00-10:00 AM of each day) for 5 consecutive days (Day 1-5). Mice feces were collected at Day 0, 6 and 13, respectively, at 15:00-17:00 PM of each day. Fecal samples were stored at -80 ^{o}C before further analysis. PE, *P. Chinense* extract. (B) Sob and (C) Shannon index of colonic microbiota. Ctrl, control group; PE_R, mice with PE treatment afer a 7-day drug-free recovery. (D) Partial least squares discriminant analysis (PLS-DA) and (E) principal co-ordinates analysis (PCoA) of all groups. (F) Phylum difference among Ctrl, PE and PE_R groups. Data are expressed as mean with SD, n=7-10 per group. *$p < 0.05$.

Figure 4. (A) Linear discriminant analysis (LDA) score and LDA effect size (LEfSe) analysis (B) in the Ctrl, PE and PE_R groups. p, phylum; c, class; o, order; f, family; g, genus. (C) Generic differences among groups by heatmap. (D) Generic differences in *norank_f_Muribaculaceae*, *Rikenellaceae_RC9_gut_group*, *Prevotellaceae_UCG-001*, *Bacteroides*, *Akkermansia*, *Ruminiclostridium*, *Ruminococcaceae_UCG-010*, *Ruminococcaceae_NK4A214_group*, *norank_Ruminococcaceae*, *Ruminococcaceae_UCG-009*, *Alistipes* and *Odoribacter* among groups. Data are expressed as mean with SD. *$p < 0.05$. Functional features of the resulting bacterial communities with *P. chinense* treatment predicted by Tax4Fun (E & F). Changes in Kyoto Encyclopedia of Genes and Genomes (KEGG) pathways are shown at different levels, (E) and (F). Data are expressed as mean with SD. *$p < 0.05$.

Figure 5. Effects of *P. chinense* treatment on (A) plasma superoxide dismutase (SOD), as well as (B) total antioxidant capacity (T-AOC), (C) catalase (CAT) activity, (D)

glutathione peroxidase (GSH-Px) activity and (E) glutathione (GSH) level in mouse liver. *$p < 0.05$, **$p < 0.01$.

Supplementary materials

Supplementary Table 1. MRM parameters for detection of each analyte.

Supplementary Table 2. Linearity, LODs and LOQs of each analyte.

Supplementary Table 3. Precisions, accuracy, stability and recovery of each analyte.

Supplementary Figure 1. Rarefaction curves of Sob (A) and Shannon (B) index.

Supplementary Figure 2. Species difference of *Bacteroides acidifaciens* (A) and *B. sartorii* (B) in different groups. *$p < 0.05$, compared with other groups.

Author contribution:

Xu Wu and Shengpeng Wang: Conceptualization, Supervision, Writing-Original draft preparation, Methodology, Funding acquisition

Jianhua Yin, Wei Ren, and Huimin Huang: Data curation, Methodology, Validation, Investigation

Xu Wu, Bin Wei, Yongshun Ma and Zhangang Xiao: Visualization, Methodology

Xiaoxiao Wu, Mingxing Li, Anqi Wang, Jing Shen, Yueshui Zhao, Fukuan Du, and Huijiao Ji: Visualization, Writing, Editing

Parham Jabbarzadeh Kaboli, Zhuo Zhang, Chi Hin Cho and Yitao Wang: Writing-Reviewing and Editing

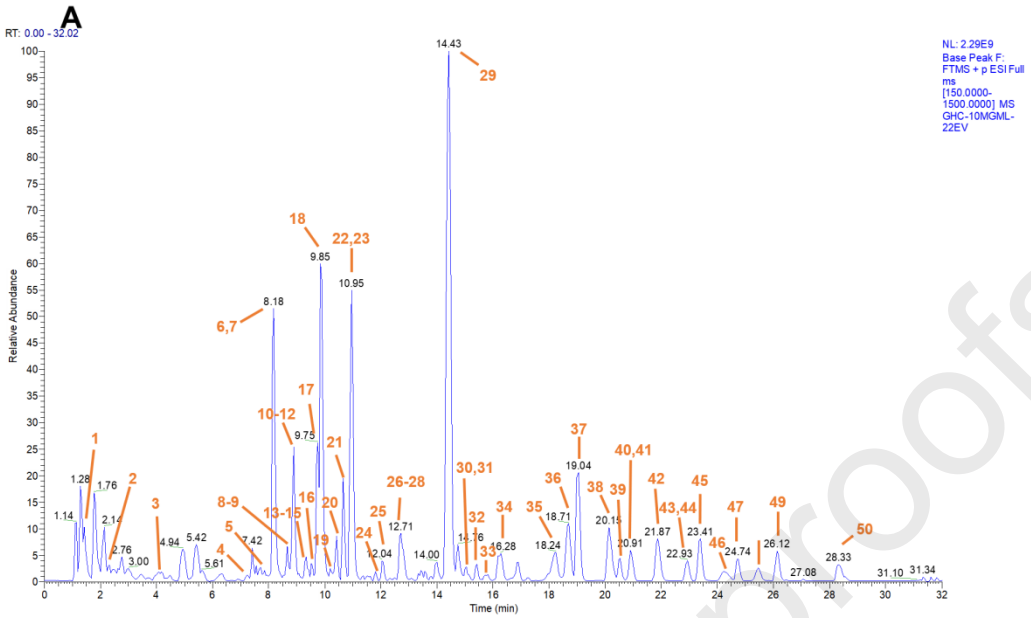

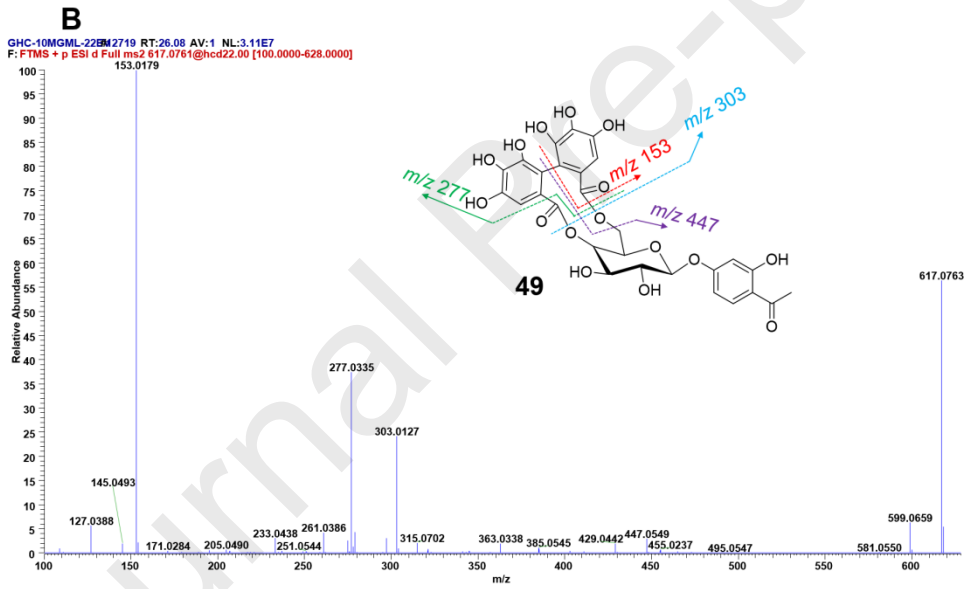

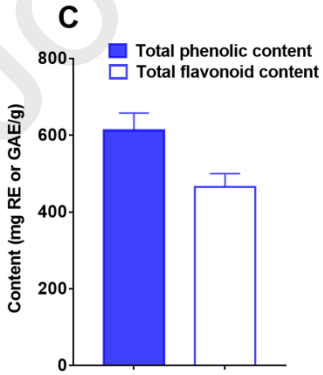

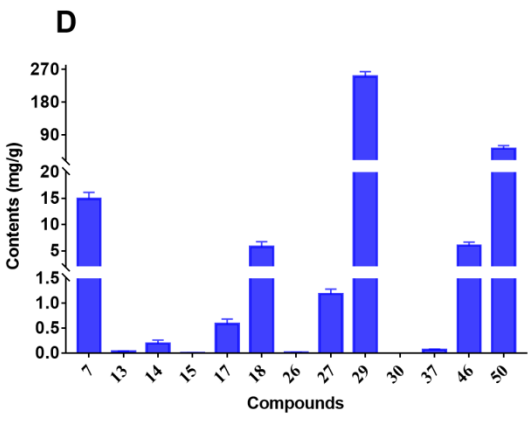

Figure 1. (A) Base-peak UPLC-HR-MS chromatogram of *P. Chinense* extract annotated with identified constituents (**1**-**50**). (B) Fragmentation of compound **49** based on MS/MS spectrum. (C) Total flavonoid and phenolic contents of *P. Chinense* extract. (D) Quantitative results of 13 polyphenols (**7**, **13**, **14**, **15**, **17**, **18**, **26**, **27**, **29**, **30**, **37**, **46**, and **50**) in *P. Chinense* extract.

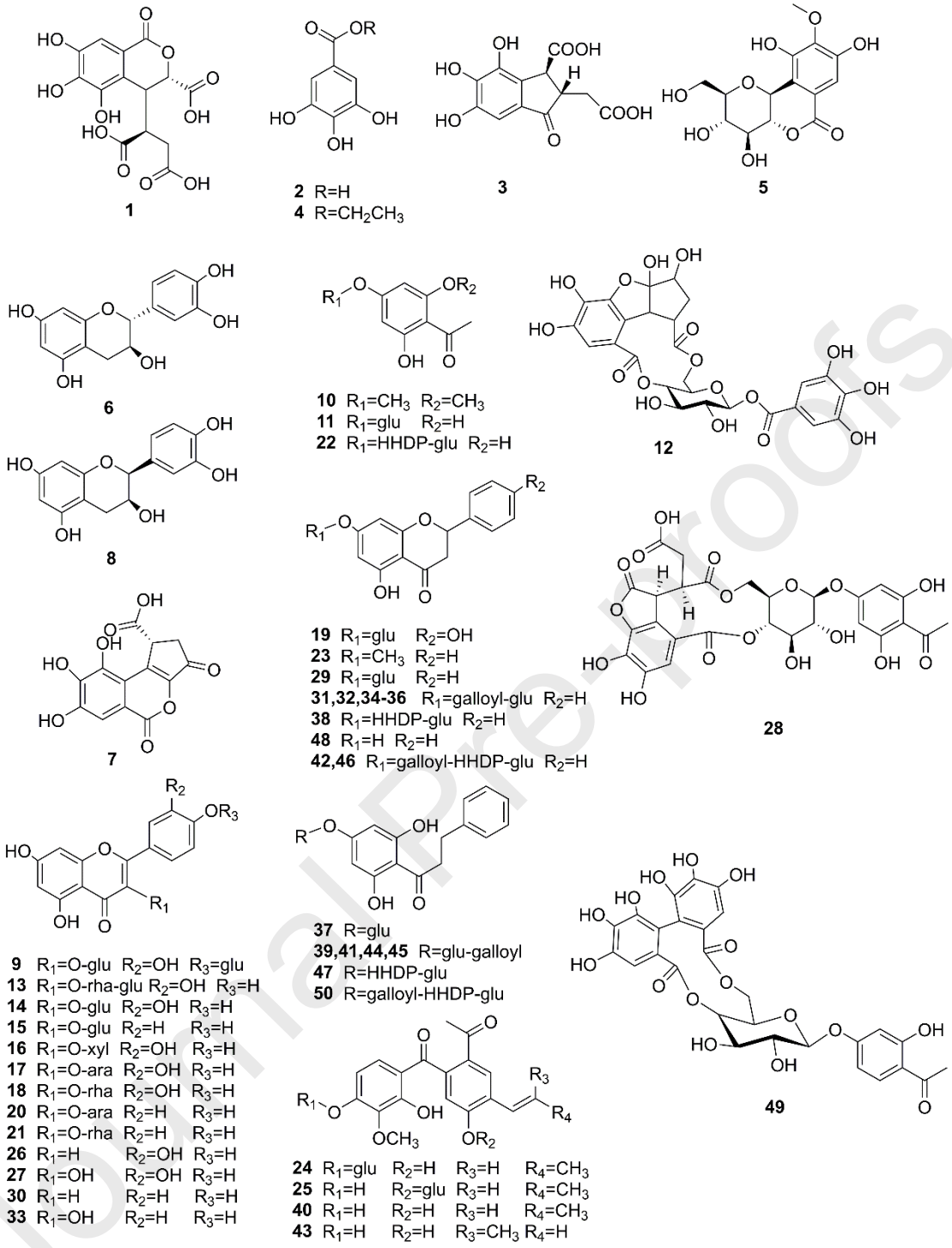

Figure 2. The structure of identified polyphenols from *P. Chinense* extract. HHDP, hexahydroxydiphenoyl; glu, glucose; rha, rhamnose; xyl, xylose; ara, arabinfuranose.

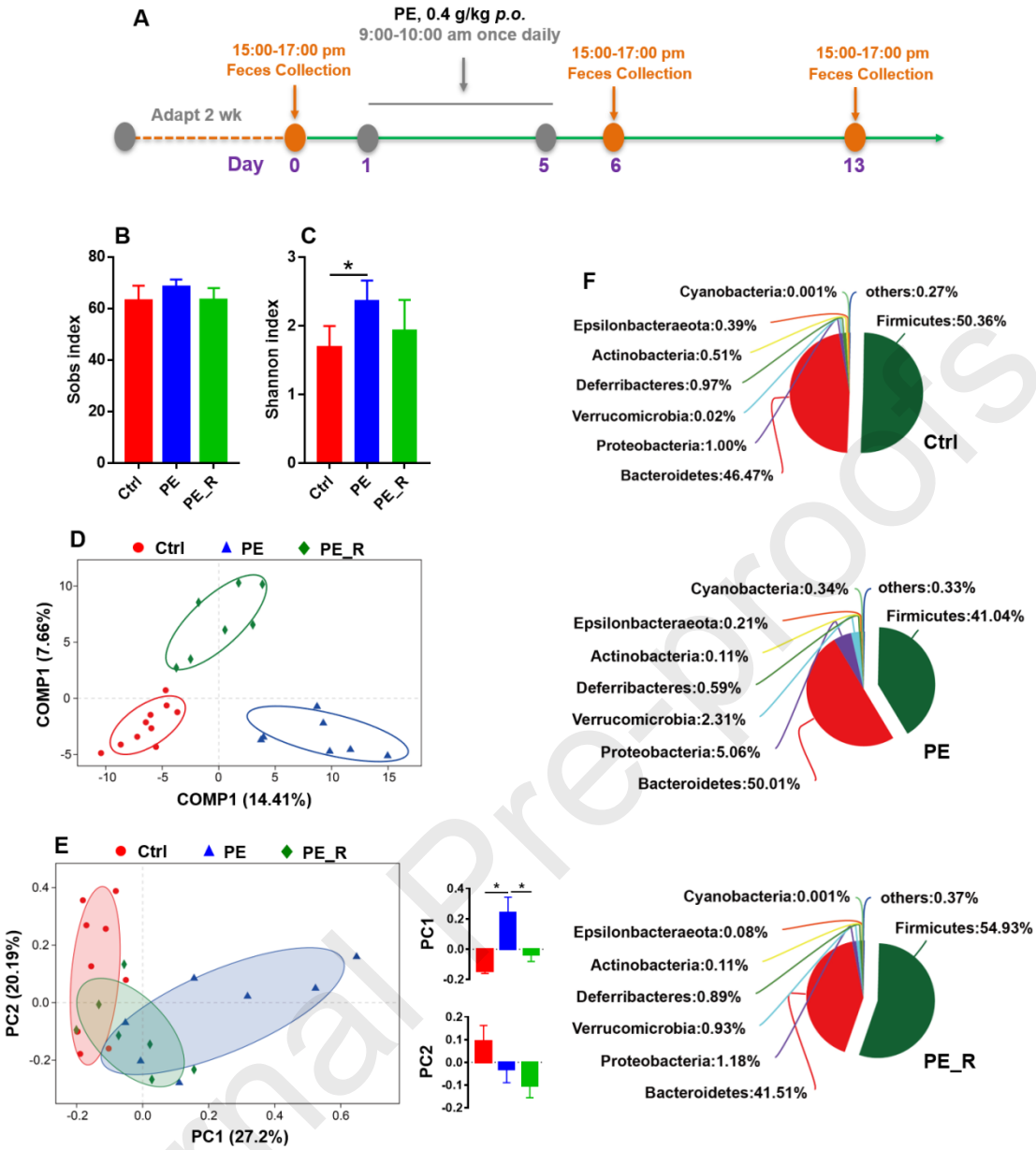

Figure 3. Structural modulation of gut microbiota by *P. chinense* in mice. (A) Schematic illustration of experimental procedures. Male C57BL/6J mice were adapted in SPF-grade animal house for two weeks before conducting experiment. Mice were orally given PE at 0.4 g/kg once daily (at 9:00-10:00 AM of each day) for 5 consecutive days (Day 1-5). Mice feces were collected at Day 0, 6 and 13, respectively, at 15:00-17:00 PM of each day. Fecal samples were stored at -80 °C before further analysis. PE, *P. Chinense* extract. (B) Sob and (C) Shannon index of colonic microbiota. Ctrl, control group; PE_R, mice with PE treatment afer a 7-day drug-free recovery. (D) Partial least squares discriminant analysis (PLS-DA) and (E) principal co-ordinates analysis (PCoA)

of all groups. (F) Phylum difference among Ctrl, PE and PE_R groups. Data are expressed as mean with SD, n=7-10 per group. *$p < 0.05$.

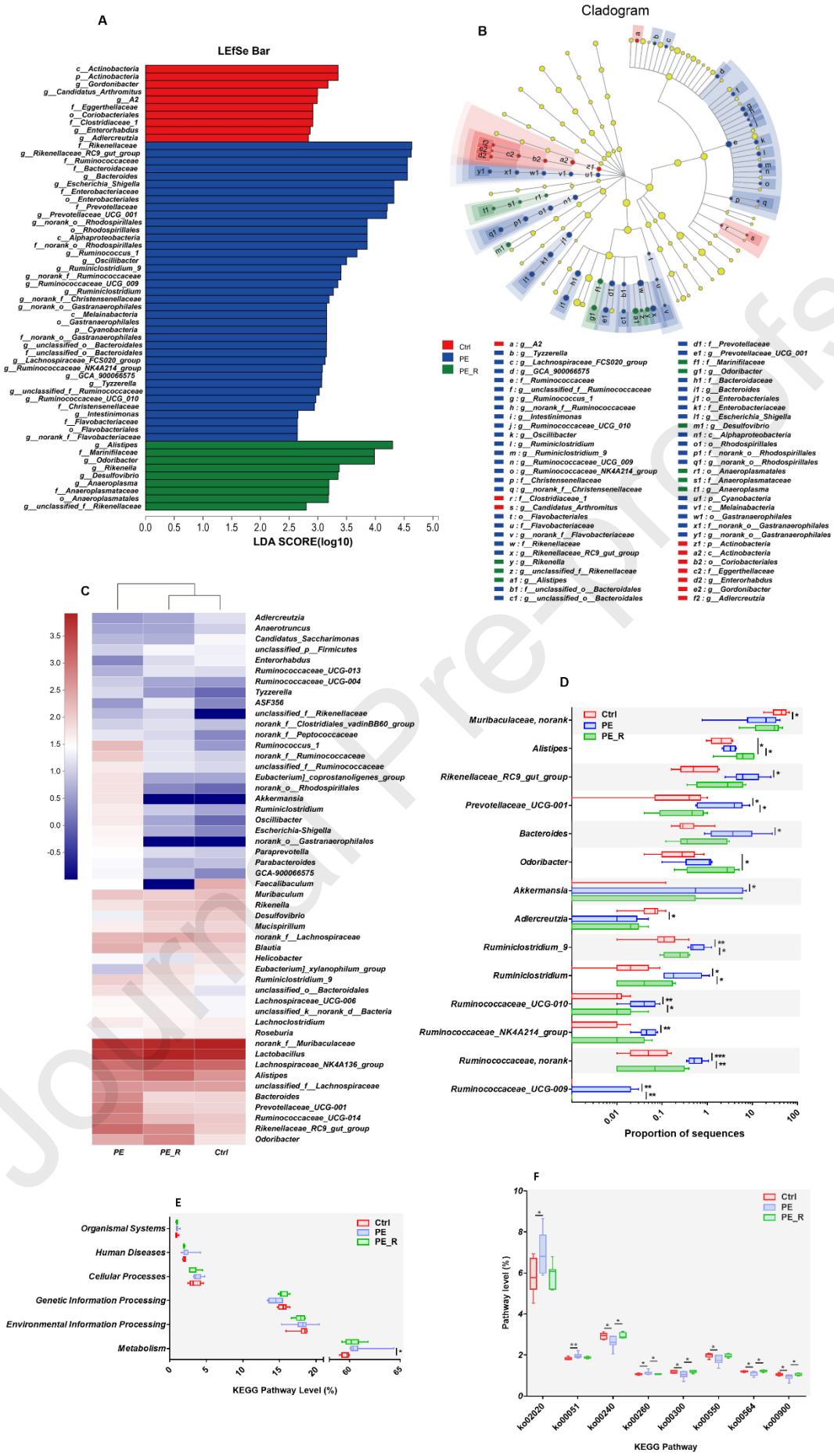
A
LEfSe Bar
c__Actinobacteria
p__Actinobacteria
g__Gordonibacter
g__Candidatus_Arthromitus
g__A2
f__Eggerthellaceae
o__Coriobacteriales
f__Clostridiaceae_1
g__Enterorhabdus
g__Adlercreutzia
f__Rikenellaceae
g__Rikenellaceae_RC9_gut_group
f__Ruminococcaceae
f__Bacteroidaceae
g__Bacteroides
g__Escherichia_Shigella
f__Enterobacteriaceae
o__Enterobacteriales
f__Prevotellaceae
g__Prevotellaceae_UCG_001
g__norank_o__Rhodospirillales
o__Rhodospirillales
c__Alphaproteobacteria
f__norank_o__Rhodospirillales
g__Ruminococcus_1
g__Oscillibacter
g__Ruminiclostridium_9
g__norank_f__Ruminococcaceae
g__Ruminococcaceae_UCG_009
g__Ruminiclostridium
g__norank_f__Christensenellaceae
g__norank_o__Gastranaerophilales
c__Melainabacteria
o__Gastranaerophilales
p__Cyanobacteria
f__norank_o__Gastranaerophilales
g__unclassified_o__Bacteroidales
f__unclassified_o__Bacteroidales
g__Lachnospiraceae_FCS020_group
g__Ruminococcaceae_NK4A214_group
g__GCA_900066575
g__Tyzzerella
g__unclassified_f__Ruminococcaceae
g__Ruminococcaceae_UCG_010
f__Christensenellaceae
g__Intestinimonas
f__Flavobacteriaceae
o__Flavobacteriales
g__norank_f__Flavobacteriaceae
g__Alistipes
f__Marinifilaceae
g__Odoribacter
g__Rikenella
g__Desulfovibrio
g__Anaeroplasma
f__Anaeroplasmataceae
o__Anaeroplasmatales
g__unclassified_f__Rikenellaceae
0.0 0.5 1.0 1.5 2.0 2.5 3.0 3.5 4.0 4.5 5.0
LDA SCORE(log10)
B
Cladogram
Ctrl
PE
PE_R
a : g__A2
b : g__Tyzzerella
c : g__Lachnospiraceae_FCS020_group
d : g__GCA_900066575
e : f__Ruminococcaceae
f : g__unclassified_f__Ruminococcaceae
g : g__Ruminococcus_1
h : g__norank_f__Ruminococcaceae
i : g__Intestinimonas
j : g__Ruminococcaceae_UCG_010
k : g__Oscillibacter
l : g__Ruminiclostridium
m : g__Ruminiclostridium_9
n : g__Ruminococcaceae_UCG_009
o : g__Ruminococcaceae_NK4A214_group
p : f__Christensenellaceae
q : g__norank_f__Christensenellaceae
r : f__Clostridiaceae_1
s : g__Candidatus_Arthromitus
t : o__Flavobacteriales
u : f__Flavobacteriaceae
v : g__norank_f__Flavobacteriaceae
w : f__Rikenellaceae
x : g__Rikenellaceae_RC9_gut_group
y : g__Rikenella
z : g__unclassified_f__Rikenellaceae
a1 : g__Alistipes
b1 : f__unclassified_o__Bacteroidales
c1 : g__unclassified_o__Bacteroidales
d1 : f__Prevotellaceae
e1 : g__Prevotellaceae_UCG_001
f1 : f__Marinifilaceae
g1 : g__Odoribacter
h1 : f__Bacteroidaceae
i1 : g__Bacteroides
j1 : o__Enterobacteriales
k1 : f__Enterobacteriaceae
l1 : g__Escherichia_Shigella
m1 : g__Desulfovibrio
n1 : c__Alphaproteobacteria
o1 : o__Rhodospirillales
p1 : f__norank_o__Rhodospirillales
q1 : g__norank_o__Rhodospirillales
r1 : o__Anaeroplasmatales
s1 : f__Anaeroplasmataceae
t1 : g__Anaeroplasma
u1 : p__Cyanobacteria
v1 : c__Melainabacteria
w1 : o__Gastranaerophilales
x1 : f__norank_o__Gastranaerophilales
y1 : g__norank_o__Gastranaerophilales
z1 : p__Actinobacteria
a2 : c__Actinobacteria
b2 : o__Coriobacteriales
c2 : f__Eggerthellaceae
d2 : g__Enterorhabdus
e2 : g__Gordonibacter
f2 : g__Adlercreutzia
C
Adlercreutzia
Anaerotruncus
Candidatus_Saccharimonas
unclassified_p__Firmicutes
Enterorhabdus
Ruminococcaceae_UCG-013
Ruminococcaceae_UCG-004
Tyzzerella
ASF356
unclassified_f__Rikenellaceae
norank_f__Clostridiales_vadinBB60_group
norank_f__Peptococcaceae
Ruminococcus_1
norank_f__Ruminococcaceae
unclassified_f__Ruminococcaceae
Eubacterium]_coprostanoligenes_group
norank_o__Rhodospirillales
Akkermansia
Ruminiclostridium
Oscillibacter
Escherichia-Shigella
norank_o__Gastranaerophilales
Paraprevotella
Parabacteroides
GCA-900066575
Faecalibaculum
Muribaculum
Rikenella
Desulfovibrio
Mucispirillum
norank_f__Lachnospiraceae
Blautia
Helicobacter
Eubacterium]_xylanophilum_group
Ruminiclostridium_9
unclassified_o__Bacteroidales
Lachnospiraceae_UCG-006
unclassified_k__norank_d__Bacteria
Lachnoclostridium
Roseburia
norank_f__Muribaculaceae
Lactobacillus
Lachnospiraceae_NK4A136_group
Alistipes
unclassified_f__Lachnospiraceae
Bacteroides
Prevotellaceae_UCG-001
Ruminococcaceae_UCG-014
Rikenellaceae_RC9_gut_group
Odoribacter
PE
PE_R
Ctrl
D
Muribaculaceae, norank
Alistipes
Rikenellaceae_RC9_gut_group
Prevotellaceae_UCG-001
Bacteroides
Odoribacter
Akkermansia
Adlercreutzia
Ruminiclostridium_9
Ruminiclostridium
Ruminococcaceae_UCG-010
Ruminococcaceae_NK4A214_group
Ruminococcaceae, norank
Ruminococcaceae_UCG-009
Ctrl
PE
PE_R
0.01 0.1 1 10 100
Proportion of sequences
E
Organismal Systems
Human Diseases
Cellular Processes
Genetic Information Processing
Environmental Information Processing
Metabolism
Ctrl
PE
PE_R
0 5 10 15 20 60 65
KEGG Pathway Level (%)
F
Pathway level (%)
0 2 4 6 8 10
ko02020
ko00051
ko00240
ko00260
ko00300
ko00550
ko00564
ko00900
KEGG Pathway
Ctrl
PE
PE_R

Figure 4. (A) Linear discriminant analysis (LDA) score and LDA effect size (LEfSe) analysis (B) in the Ctrl, PE and PE_R groups. p, phylum; c, class; o, order; f, family; g, genus. (C) Generic differences among groups by heatmap. (D) Generic differences in *norank_f_Muribaculaceae*, *Rikenellaceae_RC9_gut_group*, *Prevotellaceae_UCG-001*, *Bacteroides*, *Akkermansia*, *Ruminiclostridium*, *Ruminococcaceae_UCG-010*, *Ruminococcaceae_NK4A214_group*, *norank_Ruminococcaceae*, *Ruminococcaceae_UCG-009*, *Alistipes* and *Odoribacter* among groups. Data are expressed as mean with SD. *$p < 0.05$. Functional features of the resulting bacterial communities with *P. chinense* treatment predicted by Tax4Fun (E & F). Changes in Kyoto Encyclopedia of Genes and Genomes (KEGG) pathways are shown at different levels, (E) and (F). Data are expressed as mean with SD. *$p < 0.05$.

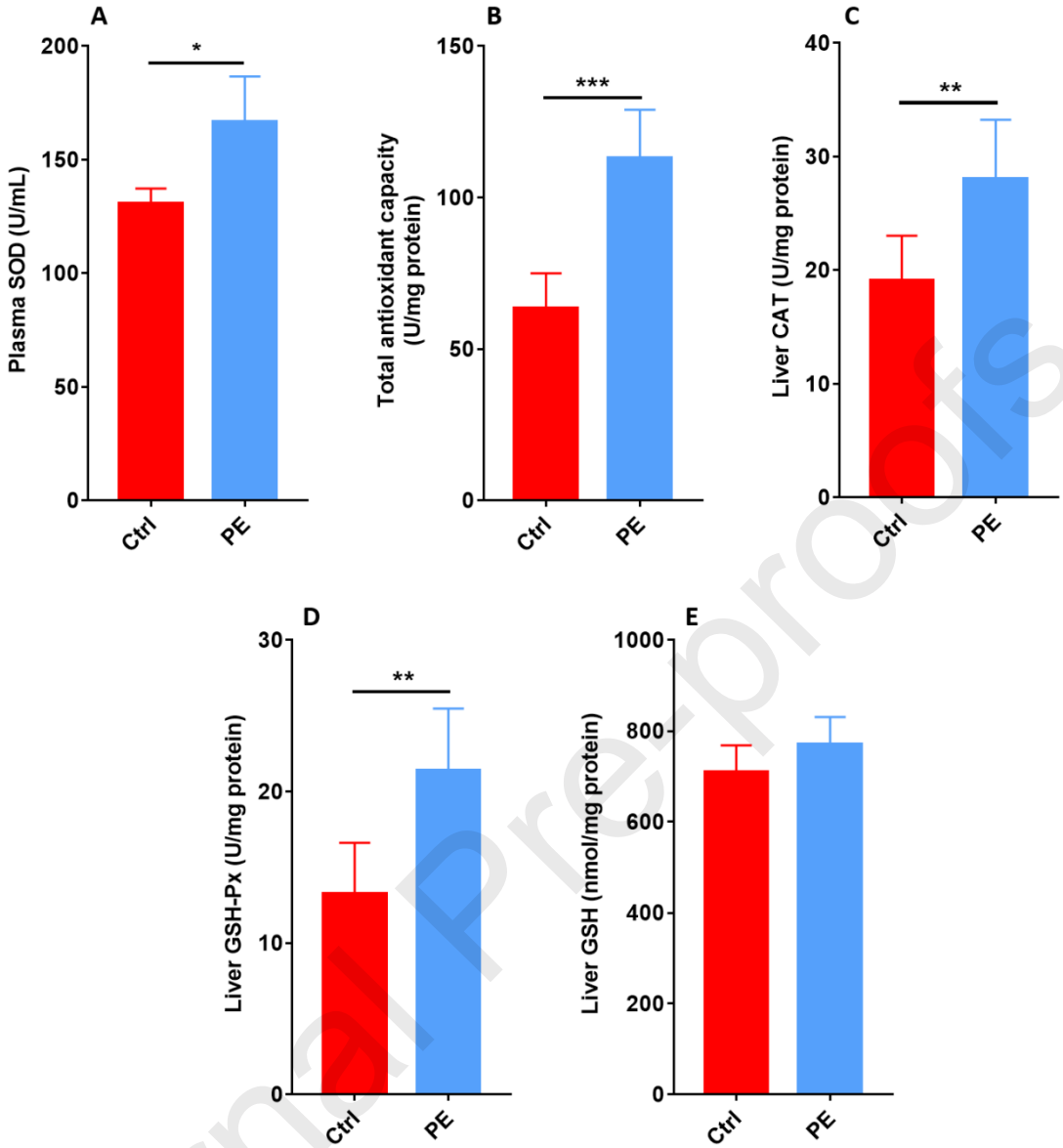

Figure 5. Effects of *P. chinense* treatment on (A) plasma superoxide dismutase (SOD), as well as (B) total antioxidant capacity (T-AOC), (C) catalase (CAT) activity, (D) glutathione peroxidase (GSH-Px) activity and (E) glutathione (GSH) level in mouse liver. *$p < 0.05$, **$p < 0.01$.

Highlights

1. Qualitative and quantitative analysis of polyphenols in *P. Chinense* by UPLC-HR-

MS and UHPLC-QqQ-MS.

2. Alteration of composition of gut microbiota by *P. Chinense*.

3. Enriched gut health-promoting bacteria by *P. Chinense* with enhanced metabolic resilience, suggesting a prebiotic effect.

4. Significantly increased antioxidant capacity *in vivo* by *P. Chinense*.